


Rapid fair sampling of the XY spin Hamiltonian with a laser simulator

Vishwa Pal ^{1,2,*} Simon Mahler ² Chene Tradonsky,² Asher A. Friesem,² and Nir Davidson²

¹*Department of Physics, Indian Institute of Technology Ropar, Rupnagar 140001, Punjab, India*

²*Department of Physics of Complex Systems, Weizmann Institute of Science, Rehovot 7610001, Israel*



(Received 26 December 2019; accepted 11 June 2020; published 2 July 2020)

Coupled oscillators such as lasers, optical parametric oscillators, and Bose-Einstein-condensate polaritons can rapidly and efficiently dissipate into a stable phase-locked state that can be mapped onto the minimal energy (ground state) of classical spin Hamiltonians. However, for degenerate or near-degenerate ground-state manifolds, statistical fair sampling is required to obtain complete knowledge of the minimal-energy state, which needs many repetitions of simulations under identical conditions. We show that with dissipatively coupled lasers such fair sampling can be achieved rapidly and accurately by exploiting the many longitudinal modes of each laser to form an ensemble of identical but independent simulators, acting in parallel. We fairly sampled the ground-state manifold of square, triangular, and kagome lattices by measuring their coherence function and identifying manifolds composed of single, doubly degenerate, and highly degenerate ground states, respectively.

DOI: [10.1103/PhysRevResearch.2.033008](https://doi.org/10.1103/PhysRevResearch.2.033008)

I. INTRODUCTION

Various combinatorial optimization problems that occur, for example, in social networks, neural networks, management of large data sets, artificial intelligence, spin glass, drug discovery, protein folding, and traveling salesmen, are considered to be computationally hard problems [1,2]. Such optimization problems can be mapped into classical spin systems (Ising or XY Hamiltonian), where they are reduced to finding the global minimum of the spin Hamiltonian [3–6]. There has been significant interest in building efficient simulators that are based on physical systems, and recently, some have been realized. These include simulators that involve coupled lasers [7,8], Bose-Einstein-condensate (BEC) polaritons [3], and optical parametric oscillators (OPOs) [2,5,9,10]. Their success relies on finding efficiently and rapidly the ground state of the spin Hamiltonian [3,10]. However, if the ground state is degenerate or nearly degenerate, the ground-state manifold must be fairly sampled in order to obtain the full knowledge of the minimal-energy state of the system, requiring many repetitions of the simulations under exactly the same conditions [6,11–13].

Generally, fair sampling corresponds to the ability to sample all the populated states of a complex system in accordance with the correct distribution function, e.g., thermal [11,12,14]. Our system is assumed to anneal into one of several (or many) degenerate ground states with equal probability, so fair sampling corresponds to accurately sampling these

degenerate ground states, which in turn provides knowledge of the ground-state manifold.

Under the assumption of constant field amplitudes, the coupled lasers are well approximated as Kuramoto phase oscillators [15]. Then the phases of the lasers can be mapped to the classical XY spins, and the ground state of the classical XY Hamiltonian can be analogous to the phase-locked steady state of the coupled lasers [7]. Unlike finding the ground state of spin systems by cooling externally, in coupled lasers the internal dissipation caused by coupling drives the lasers into a globally stable phase-locked state (minimal-loss state), identical to the ground state of the classical XY spin Hamiltonian [7,8]. The dissipatively coupled lasers were formed in a degenerate cavity laser arrangement for observing dissipative topological defects in a discrete one-dimensional ring of phased-locked lasers and for relating their formation to the Kibble-Zurek mechanism [8]. The phase-locking states of the lasers were determined by detecting the far-field intensity distributions of both positively and negatively (nearest neighbors) coupled lasers and could not be compared to the ground state of a XY spin Hamiltonian. The advantages of dissipative mechanisms were also demonstrated in OPOs and BEC polaritons simulators [2,3,10].

In this work, we present and characterize a simulator for the XY spin Hamiltonian based on linearly coupled lasers that rapidly performs statistical fair sampling of its ground-state manifold by exploiting massive parallelism that is available with the lasers. Specifically, each laser has approximately 250 longitudinal modes that form an ensemble of approximately 250 identical but independent simulators of the XY spin Hamiltonian. This provides a massive parallelism that enables rapid and accurate fair sampling of the ground-state manifold. We directly measure the statistical average of spin ordering (magnetization) of the ground-state manifold by measuring coherence between the lasers in different lattice geometries having single, double, and many degenerate ground states. For a triangular lattice with positive coupling, we measure

*Corresponding author: vishwa.pal@iitrpr.ac.in

Published by the American Physical Society under the terms of the [Creative Commons Attribution 4.0 International](https://creativecommons.org/licenses/by/4.0/) license. Further distribution of this work must maintain attribution to the author(s) and the published article's title, journal citation, and DOI.

the long-range uniform coherence function, indicating a non-degenerate single ground state, which could also be inferred from the sharp peaks that were observed in the far-field diffraction pattern [7,8]. For a triangular lattice with negative coupling, we measure an oscillatory coherence function, indicating a doubly degenerate ground state, which could not be directly inferred from the far-field diffraction pattern. Finally, for a kagome lattice with negative coupling, we measure an exponentially decaying coherence function, which manifests the degenerate ground states due to geometric frustration [7].

When the internal phases of each laser are varied, the coherence function is modified into a directional coherence function, corresponding to new stripe phase ordering. All these experimental results agree with a theoretical model based on statistical fair sampling of the ground-state manifold. We also observe and explain an intriguing ensemble average difference of π between the phases of nearest-neighbor lasers that are negatively coupled, even in triangular lattices.

II. EXPERIMENTAL ARRANGEMENT AND PROCEDURES

The experimental arrangement, lattice configurations, and representative results are presented in Fig. 1. Our coupled lasers in lattices are formed in a degenerate cavity shown schematically in Fig. 1(a) (yellow shaded region). It is composed of two mirrors, two lenses in a 4f telescope, a mask containing several hundred circular holes in different lattice geometries, and a Nd:yttrium aluminum garnet gain medium pumped by a 100- μ s pulsed xenon flash lamp. The intracavity 4f telescope ensures that any field distribution at the mask plane is imaged onto itself after every round trip. Accordingly, each hole on the mask defines an independent individual laser [7,8,16]. Each laser lases with a nearly pure single Gaussian transverse mode (forced by a 200- μ m-diameter circular aperture located in the Fourier plane of the intracavity telescope) and approximately 250 longitudinal modes that are common to all lasers due to the degenerate cavity condition. The number of lasing longitudinal modes in the degenerate cavity can be determined by the ratio of the total laser bandwidth (~ 32 GHz) over the free spectral range of the cavity (spacing between the successive longitudinal modes, ~ 128 MHz), which yields ~ 250 longitudinal modes (as verified experimentally in [17]).

It should be noted that due to gain competition only ~ 250 longitudinal modes lase inside the laser cavity, indicating some coupling between them. However, the gain is located in the near-field plane, where all ground states have the same intensity distributions and hence the same gain. Thus, there is no distinction between the ground states, and it does not bias the sampling of ground-state manifold. Conversely, biasing in sampling occurs when a nonlinear element is located at the far-field plane, where different ground states have different intensity distributions and hence different nonlinear responses [18].

We verified that lasers are independent by showing that each laser is incoherent with all the other lasers (see Appendix A). Coupling between adjacent lasers is introduced by shifting mirror M_1 a distance d of quarter-Talbot length away from the mask [19]. Such a distance results in negative coupling between adjacent lasers, corresponding to

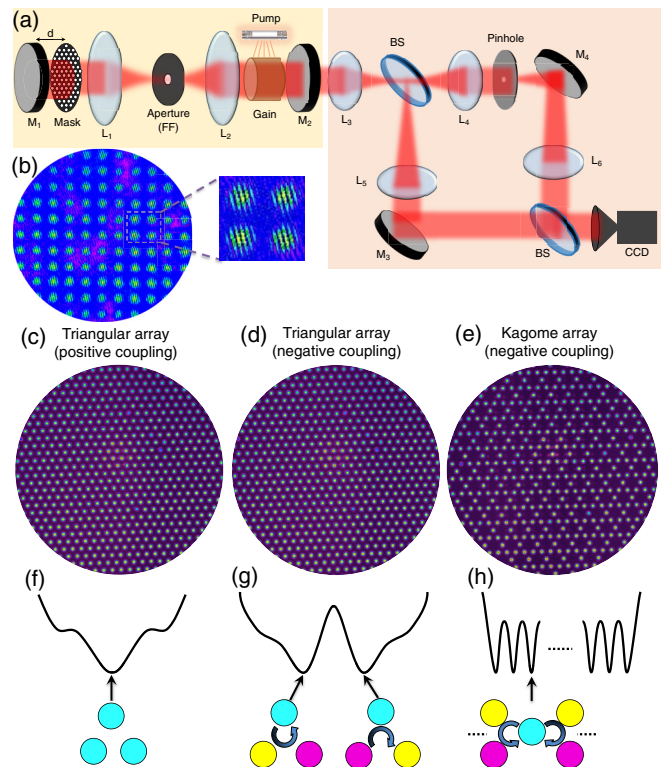


FIG. 1. Experimental arrangement, lattice geometries, and representative results. (a) Schematic of a degenerate cavity laser (shaded in yellow) that forms and phase locks lasers in different lattice geometries, together with a Mach-Zehnder interferometer (shaded in orange) for analyzing the coherence between the lasers. (b) Experimentally measured interference pattern when a single reference laser interferes with itself and with all the other lasers in the square lattice. Experimental near-field intensity patterns for (c) the triangular lattice with positive coupling, (d) the triangular lattice with negative coupling, and (e) the kagome lattice with negative coupling. (f) Landscape with a single ground state, corresponding to the in-phase locked triangular lattice. (g) Landscape with two degenerate ground states, corresponding to vortex and antivortex states of the out-of-phase locked triangular lattice. (h) Landscape with highly degenerate ground states, corresponding to 2^n states (n is the number of triangles) in the out-of-phase locked kagome lattice. Note that for $n = 2$, only one state out of four states is shown. Different colors of the lasers denote different values of the phases. Cyan = 0, yellow = $2\pi/3$, and pink = $-2\pi/3$. M_1 and M_2 denote high-reflectivity and partial-reflectivity cavity mirrors, and M_3 and M_4 denote high-reflectivity mirrors. L_1 , L_2 , L_3 , L_4 , L_5 , and L_6 indicate plano-convex lenses, BS is the beam splitter, and CCD indicates the camera.

antiferromagnetic ordering of classical XY spins [20]. Alternatively, d of half-Talbot length combined with Fourier filtering provides positive coupling between adjacent lasers, corresponding to ferromagnetic ordering [21].

The coherence between the lasers is described as [22]

$$V_{ij} = \sqrt{\langle \cos(\phi_{ij}) \rangle^2 + \langle \sin(\phi_{ij}) \rangle^2}, \quad (1)$$

where $\phi_{ij} = \phi_i - \phi_j$, ϕ_i and ϕ_j are the phases of lasers i and j mapped to the orientation angle of spins i and j , and $\langle \cdot \rangle$ denotes averaging over the ensemble of simulators, which is achieved simultaneously with our coupled lasers.

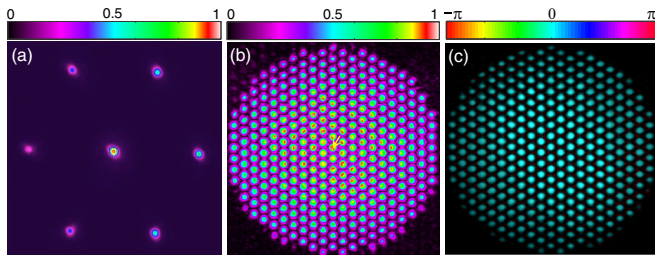


FIG. 2. Positively coupled lasers in a triangular lattice. (a) Ensemble-averaged far-field diffraction pattern, indicating long-range in-phase ordering. (b) The coherence calculated from the interference pattern measured by the Mach-Zehnder interferometer, also indicating long-range phase ordering. (c) The phases of lasers calculated from the measured interference pattern, indicating long-range in-phase ordering throughout the lattice. The yellow arrow in (b) denotes the location of the reference laser (it is the same in other figures).

The coherence between the lasers [Eq. (1)] is measured using a Mach-Zehnder interferometer, shown in Fig. 1(a) (orange shaded region). The output of lasers from the degenerate cavity splits into two channels at the first beam splitter. In one channel, the output of all the lasers is imaged directly onto the CCD camera. In the other channel, a single reference laser is selected using a pinhole with a size of $50 \mu\text{m}$, and then its light is expanded so that it fully overlaps and interferes with the light of all the lasers with a second beam splitter on the camera. Thus, a single selected reference laser interferes with itself and with all the other lasers. A small tilt between the two channels provides few interference fringes for each laser [exemplified in Fig. 1(b) for a square lattice] from which the fringe visibility (coherence) and shift (phase difference) are obtained for all lasers by digital Fourier analysis. The measured coherence function is normalized such that the coherence of the reference laser with itself is 1. We also measure the far-field diffraction pattern of the lasers in the lattice that corresponds to the ensemble-averaged structure factor of the lattice [7] where sharp Bragg peaks indicate long-range phase ordering between the lasers.

III. FAIR SAMPLING OF THE GROUND-STATE MANIFOLD

Using the experimental arrangement shown in Fig. 1, we performed a series of experiments to demonstrate fair sampling of the ground-state manifold in square, triangular, and kagome lattices. We first phase locked about 320 lasers with positive coupling in a triangular lattice [Fig. 1(c)]. The results in Fig. 2 represent an ensemble averaging over about 250 independent realizations, each corresponding to a different longitudinal mode.

Figure 2(a) shows the far-field diffraction pattern of the lasers, where the sharp Bragg peaks indicate long-range in-phase ordering. The measured coherence [Fig. 2(b)] of the lasers also evidences long-range phase ordering and barely decays with distance from the reference laser. There are six straight directions with respect to the reference laser, in which, by symmetry, the coherence decay should be identical. For the

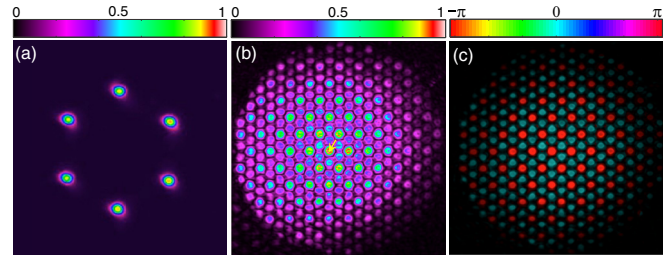


FIG. 3. Negatively coupled lasers in a triangular lattice. (a) Ensemble-averaged far-field diffraction pattern containing two states (vortex and antivortex). (b) The coherence calculated from the measured interference pattern, showing high coherence every three lasers in the ensemble average. (c) The phases of lasers calculated from the measured interference pattern, showing a phase difference of π (from the reference laser) between nearest neighbors in the ensemble average.

statistical analysis, the coherence is averaged over all these six directions (see Fig. 6 below and Appendix D) to quantify the accuracy of fair sampling. Finally, Fig. 2(c) shows the measured phases of the lasers (relative to the reference laser), confirming in-phase ordering throughout the lattice. The observed long-range in-phase ordering shows that the entire ensemble of experiments (realized by multiple longitudinal modes) converged to the same nondegenerate ground state, as expected from its single minimal-loss manifold illustrated in Fig. 1(f). This convergence is analogous to perfect ferromagnetic spin ordering of XY spins. We obtained long-range (out-of-phase) ordering also for a square lattice with negative coupling [Fig. 1(b)] that has the same single minimal-loss manifold (see Appendix B).

Next, we investigated the triangular lattice of about 320 negative coupled lasers. Figure 3(a) shows the far-field diffraction pattern, which is composed of six sharp Bragg peaks that indicate long-range phase ordering. Three of these Bragg peaks correspond to a vortex state illustrated as the left ground state in Fig. 1(g), and other three peaks correspond to an antivortex state illustrated as the right ground state in Fig. 1(g) [7,21,23]. These two degenerate ground states have (by symmetry) equal probability to be populated by the ensemble of experiments realized by the multiple longitudinal modes, as indicated by the equal intensity of their Bragg peaks in the diffraction pattern in Fig. 3(a).

The coexistence of the two degenerate ground states has remarkable consequences for the measured coherence function that oscillates where the coherence with respect to the reference laser revives every three lasers [Fig. 3(b)]. This surprising behavior can be understood by noting that for the nearest-neighbor (NN) and next-nearest-neighbor (NNN) lasers, the vortex and antivortex states differ by $\pm 2\pi/3$. So their interference fringes are shifted and, as a result of ensemble averaging, reduce the coherence to 50%. However, for the next-next-nearest-neighbor (NNNN) laser these two states have the same relative phase, yielding a coherence of 100% (and then the same 50%, 50%, 100% coherence periodicity is repeated). Figure 3(c) shows the ensemble-averaged phases of the lasers, indicating a phase difference of π (from the reference laser) between the nearest neighbors. This is analogous

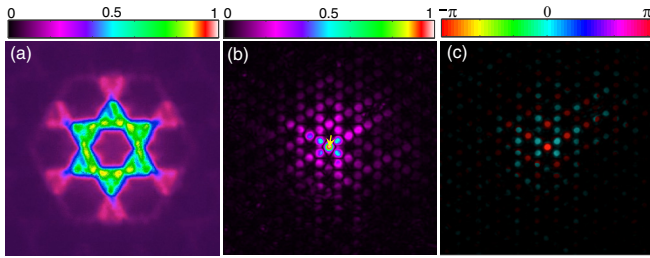


FIG. 4. Negatively coupled lasers in a kagome lattice. (a) Ensemble-averaged far-field diffraction pattern, containing many vortex and antivortex states. (b) The coherence calculated from the measured interference pattern, showing exponential decaying behavior in the ensemble average. (c) The phases of the lasers calculated from the measured interference pattern, showing a phase difference of π (from the reference laser) between nearest neighbors in the ensemble average.

to XY spin systems, where XY spins oriented at $+2\pi/3$ and $-2\pi/3$ yield a spin with magnitude one half oriented at π in the ensemble averaging.

The XY spin Hamiltonian on a kagome lattice [Fig. 1(e)] exhibits highly nontrivial features such as geometric frustration that arises due to massive degeneracy in its ground state [7,24,25]. The degeneracy scales exponentially with the system size; thus, performing fair sampling is a computationally hard problem [6]. The results for fair sampling in a kagome lattice with about 350 negatively coupled lasers are shown in Fig. 4.

Figure 4(a) shows the ensemble-averaged far-field diffraction pattern that consists of large-area Bragg lobes (rather than sharp peaks), indicating the lack of long-range phase ordering, in agreement with the theoretical results [7,25]. Specifically, in a kagome lattice, each triangle of lasers can randomly find either the vortex or the antivortex degenerate ground state with equal probability, thereby suppressing long-range phase ordering. Figure 4(b) shows a rapid decay of coherence, indicating again the lack of long-range phase ordering. There are four “diagonal” directions in which, by symmetry, the coherence decay should be identical and other directions (e.g., horizontal and vertical) in which decay is more rapid due to the absence of lasers. Within the four diagonal directions, the exact symmetry is broken by the nonuniformity of the laser amplitudes and coupling between them. The statistical analysis of these nonuniformities (see Appendix D) quantifies the accuracy in which our results agree with fair sampling. The coherence function can be quantitatively determined by calculating the probability distribution of states that have relative phase differences $\pm 2\pi/3$ or 0 with respect to the reference laser. For example, for NN, equal-probability states with relative phases of $\pm 2\pi/3$ reduce the coherence to 50%. For NNN and NNNN, the coherence is reduced to 25% and 12.5%, respectively [26]. More generally, at a distance n from the reference laser, the coherence continues to drop exponentially as $1/2^n$. Figure 4(c) shows the ensemble-averaged phase ordering, indicating a π phase difference (from the reference laser) between the nearest neighbors, analogous to the XY spin system.

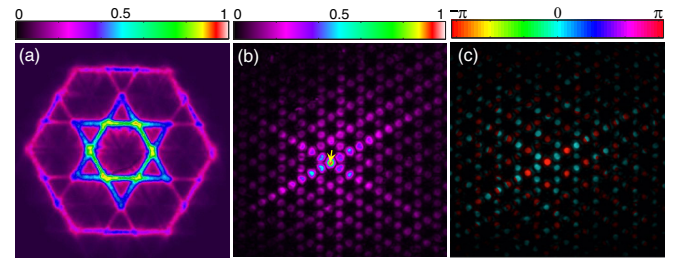


FIG. 5. Negatively coupled lasers in a kagome lattice with a large-diameter intracavity Fourier aperture. (a) Ensemble-averaged far-field diffraction pattern. (b) The coherence calculated from the measured interference pattern. (c) The phases of the lasers calculated from the measured interference pattern.

We also investigated the coherence of the kagome lattice when the intracavity Fourier aperture has a large diameter, so that each laser is no longer a pure TEM_{00} mode and contains fine internal features which diffract faster and can generate NNN coupling. The results, shown in Fig. 5, differ dramatically from those without NNN coupling in Fig. 4. Figure 5(a) presents the ensemble-averaged far-field diffraction pattern, which now consists of sharp, narrow lines indicating long-range phase ordering only along certain directions. Figure 5(b) shows the measured coherence that decays slowly along certain directions, confirming such anisotropic long-range phase ordering. Figure 5(c) shows the ensemble-averaged phases, which again indicate the relative phase difference of π (from the reference laser) between nearest neighbors. This intriguing, highly directional phase ordering is also observed in our numerical simulations (see Appendix C 1) and is accompanied by spontaneous intensity-pattern formation as in the stripe phase of ultracold atoms [27].

Finally, we have quantified the coherence as a function of distance from the reference laser and compared the experimental results to the analytical ones, as shown in Fig. 6 (and in Appendix C 2). The distance from the reference laser is defined such that NN, NNN, and higher-order lasers are

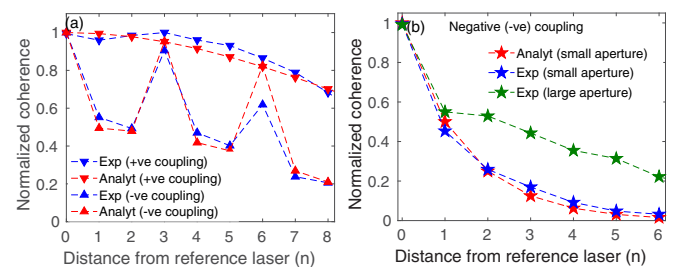


FIG. 6. The ensemble-averaged normalized coherence as a function of distance from the reference laser. (a) Normalized coherence for the positively coupled lasers (inverted blue and red triangles) and negatively coupled lasers (blue and red triangles) in a triangular lattice. For the positive coupling, the coherence is monotonic, whereas for the negative coupling the coherence shows an oscillatory behavior in agreement with the analytical results. (b) In a negatively coupled kagome lattice, normalized coherence decays exponentially for NN coupling (blue and red stars) but decays much slower with NNN coupling (green stars).

along a straight line in symmetric directions. For example, in triangular (kagome) lattices there are six (four) symmetric directions. The coherence as a function of distance from the reference laser is averaged over all these directions in each lattice geometry. Figure 6(a) shows the normalized coherence as a function of the distance from the reference laser for positively and negatively coupled lasers in a triangular lattice. For the positively coupled lasers, the coherence decays slowly and monotonically (blue and red inverted triangles). As is evident, the ensemble averaging does not reduce the coherence, indicating a single nondegenerate ground state. For the negatively coupled lasers, both the analytical and experimental coherences show an oscillatory behavior as a function of distance from the reference laser (blue and red triangles), where the coherence revives every three lasers. This loss and revival of the ensemble-averaged coherence with distance from the reference laser indicates two degenerate ground states.

Figure 6(b) shows the normalized coherence as a function of the distance from the reference laser in a kagome lattice with NN and NNN negative coupling. For NN negative coupling, the ensemble-averaged coherence decays exponentially, in agreement with the analytical results [26] (blue and red stars). The exponential decay indicates massive degeneracy in the ground state that scales exponentially with the system size due to geometric frustration [7]. For NNN coupling, the ensemble-averaged coherence decays much slower as a function of the distance from the reference laser (green stars), indicating a reduced number of degenerate ground states.

Equal sampling of the ground states in the negatively coupled triangular lattice and the kagome lattice should lead to a 0.5 normalized coherence for NN lasers. We analyze the measured coherence for all six (four) NNs in the triangular (kagome) lattices and find the average normalized coherence is 0.53 (0.53) and its standard deviation is 0.05 (0.06) (see Figs. 6 and 11). Within these deviations that are due to aberrations and noise in the experimental arrangement, our results are consistent with ideal fair sampling (for more details on the NNN coherence, see Appendixes C and D).

IV. CONCLUDING REMARKS

We presented a simulator based on dissipatively coupled lasers for rapid and efficient fair sampling of magnetic ordering of the XY spin Hamiltonian with ground-state degeneracy. The simulator exploited 250 longitudinal modes of each laser to form an ensemble of 250 identical but independent simulators to provide massive parallelism in performing statistical fair sampling. We investigated the ground-state manifold in different geometries such as square, triangular, and kagome lattices. For negative (positive) coupling, we observed a single ground state for the square (triangular) lattice, two degenerate ground states for the triangular lattice, and geometrically frustrated highly degenerate ground states for the kagome lattice. For these cases, the corresponding spatial coherence functions are either nearly uniform or oscillatory or exponentially decaying. Under certain conditions, we also observed highly directional phase ordering in a kagome lattice, indicating reduced ground-state degeneracy.

In this work, we tested the fair sampling by analyzing the ensemble-averaged coherence function. The results of our statistical analysis are in good agreement with the theoretical predictions, thus verifying our approach indeed performs fair sampling. Our simulator with rapid fair sampling of the ground-state manifold could potentially be exploited to address various combinatorial optimization problems. We plan to extend our work to study the effects of defects on the ensemble-averaged coherence in two-dimensional lattices and their influence on the ground-state manifolds.

Our experimental arrangement can also be exploited to solve optimization problems by using problem-specific near-field and far-field masks to obtain desired near-field amplitude distribution and desired coupling between the lasers. The desired near-field amplitude distribution can also be implemented by means of an electronically controlled spatial light modulator as one of the cavity mirrors [28], and arbitrary coupling between the lasers can be implemented with an optical vector multiplication arrangement to form a coupling matrix [29,30]. Fair sampling is especially important for computationally hard problems that are mapped onto spin systems with many degenerate or near-degenerate ground states.

ACKNOWLEDGMENTS

The authors acknowledge partial support from the Israel Science Foundation (ISF) (Grant No. 1881/17) and an ISIRD grant from the Indian Institute of Technology Ropar (Grant No. 9-320/2018/IITRPR/3255).

APPENDIX A: UNCOUPLED LASERS IN THE SQUARE LATTICE

Here we show that without coupling the lasers in the lattice are independent of each other. The lattices of lasers are formed in a degenerate cavity, as shown in Fig. 1(a) (shaded in yellow) in the main text. The results for the square lattice are shown in Fig. 7. Figure 7(a) shows the near-field intensity pattern of the lasers arranged in the square lattice, where the output from each laser is a Gaussian TEM_{00} mode. Figure 7(b) shows the ensemble-averaged far-field diffraction pattern that consists of a broad Gaussian distribution, which indicates that the lasers are independent of each other [7]. We also measured the interference pattern using the Mach-Zehnder interferometer shown in Fig. 1(a) (shaded in orange), where light from a single reference laser can interfere with itself and with the light from all other lasers. The results, shown in Fig. 7(c), indicate that fringes appear at only one laser site [see the inset in Fig. 7(c)], where the light from the reference laser interferes only with itself. The corresponding coherence (fringe visibility) obtained by digital Fourier analysis is shown in Fig. 7(d) as a single spot, indicating that the selected laser is coherent only with itself and not with the other uncoupled lasers. These results confirm that the lasers in the lattice are independent and fully incoherent.

APPENDIX B: COUPLED LASERS IN THE SQUARE LATTICE

Here we show the effect of coupling on the square lattice of lasers. We introduce coupling between the lasers by means

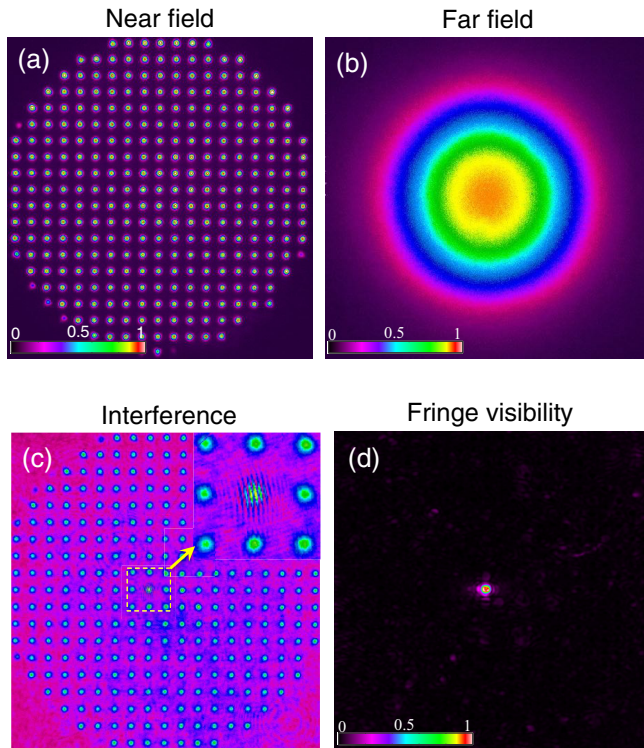


FIG. 7. Experimental results for the uncoupled lasers in a square lattice. (a) The near-field intensity pattern of lasers. (b) The far-field diffraction pattern of lasers. (c) The interference pattern when the output light from a single laser interferes with itself and with the light from all other lasers. (d) The coherence calculated from the measured interference pattern.

of Talbot diffraction [21] and then detect the effect on the output intensity distribution and coherence. The results are presented in Fig. 8. Figure 8(a) shows the ensemble-averaged far-field diffraction pattern which is composed of sharp Bragg peaks with darkness in the center, indicating a long-range out-of-phase ordering. Figure 8(b) shows the interference pattern, where fringes were detected at all the laser sites, indicating long-range phase ordering. The analyzed coherence shown in Fig. 8(c) also indicates long-range phase ordering, where it barely decays with distance from the reference laser (center laser). Finally, Fig. 8(d) shows the measured phases of the lasers (relative to the reference laser), confirming out-of-phase ordering throughout the lattice. All these results were obtained with ensemble averaging over 250 independent realizations, each corresponding to a different longitudinal mode. Accordingly, the detected long-range out-of-phase ordering provides evidence that the entire ensemble of experiments (realizations) occupies the same nondegenerate ground state. This is equivalent to perfect antiferromagnetic spin ordering of XY spins.

APPENDIX C: NUMERICAL SIMULATIONS AND ANALYTICAL RESULTS

1. Numerical simulations

Here we describe the numerical simulations that were used to verify the experimental results of negatively coupled lasers

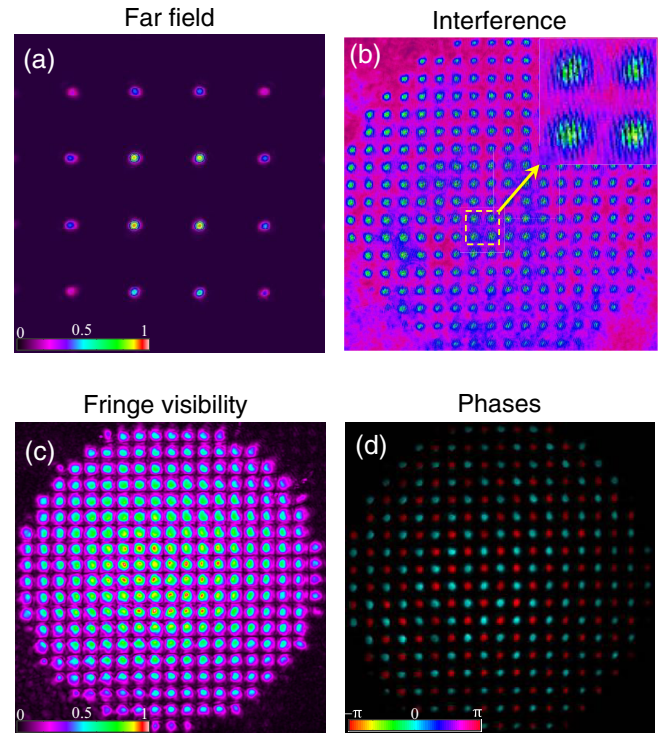


FIG. 8. Experimental results for the negatively coupled lasers in a square lattice. (a) The far-field diffraction pattern of the laser lattice. (b) The interference pattern when the output light from a single reference laser interferes with itself and with the light from all other lasers. (c) The coherence calculated from the measured interference pattern. (d) The phases of the lasers calculated from the measured interference pattern.

in a kagome lattice, shown in Figs. 4 and 5. The simulations were performed with an algorithm that combines the Fox-Li algorithm [31] and Gerchberg-Saxton algorithm [32]. The parameters for the simulations were the same as those used in the

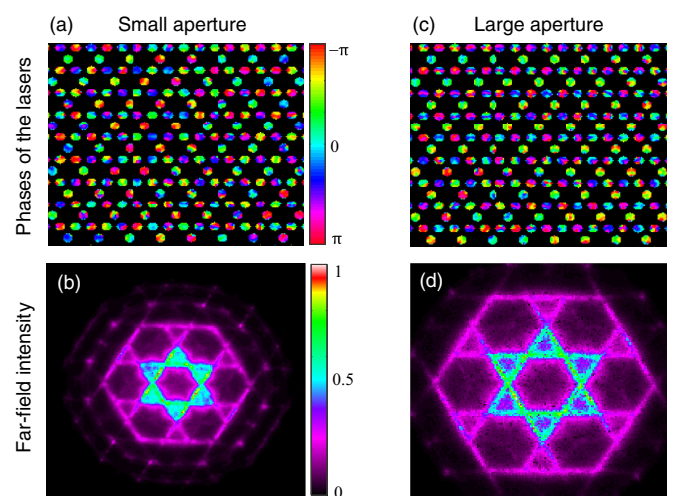


FIG. 9. Simulated phase and far-field diffraction pattern of negatively coupled lasers in a kagome lattice for two different far-field aperture radii R . The top row shows the simulated phases of the lasers, and the bottom row shows the corresponding simulated far-field diffraction patterns.

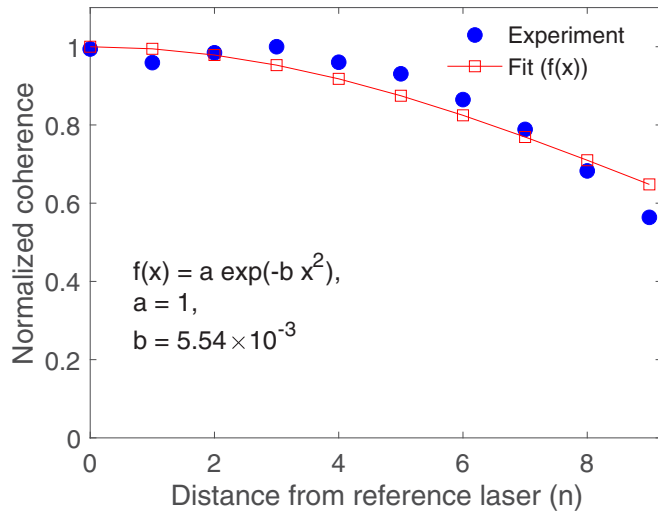


FIG. 10. Normalized coherence as a function of distance from the reference laser. The experimental visibility (blue dots) was fitted with a Gaussian decaying function (red line with squares) to extract the decay of coherence due to aberrations and noise.

experiment. The simulation results were averaged over 100 realizations (corresponding to 100 independent longitudinal modes) to perform fair sampling. The simulated results are shown in Fig. 9 for small and large far-field aperture radii R . The top row shows the simulated phases of the lasers, and the bottom row shows the corresponding far-field diffraction patterns. Note that the phases correspond to individual lasers, not the relative phase between the lasers.

For small aperture $R = 1$, Fig. 9(a) shows that the phase distribution in each laser is almost uniform (almost pure TEM_{00} mode). The far-field diffraction pattern [Fig. 9(c)] shows large-area Bragg lobes with diffusive lines similar to those in Fig. 4(a), indicating the lack of long-range phase ordering. For large aperture $R = 1.2$, the phase distribution in each laser is mostly nonuniform (no longer a pure TEM_{00} mode). The far-field diffraction pattern [Fig. 9(d)] shows sharp lines similar to those in Fig. 5(a), indicating long-range phase ordering only along certain directions.

2. Analytical results

Here we describe the method to calculate the decay of the coherence function shown in Fig. 6(a) for the triangular lattice of lasers. We attribute the decay of the measured coherence to aberrations and noise in our experimental arrangement [8]. We first fitted the measured coherence of positively coupled lasers (in-phase ordered) with a Gaussian decay function

$$f(x) = a e^{-bx^2}, \tag{C1}$$

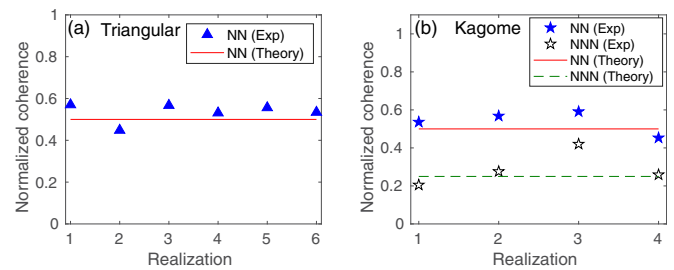


FIG. 11. The normalized coherence as a function of different realizations. (a) For NN lasers in a negatively coupled triangular lattice, the normalized coherence varies within the standard deviation of 5%. (b) For NN and NNN lasers in a negatively coupled kagome lattice, the normalized coherences vary within standard deviations of 6% and 8%.

where $a = 1$, $b = 5.54 \times 10^{-3}$, and x is the distance from the selected laser. The fitted curve is shown in Fig. 10. We multiplied the uniform coherence function [$f(x) = 1$] of the in-phase ordered triangular lattice and oscillatory coherence function of the out-of-phase ordered triangular lattice [$f(x) = 1, 0.5, 0.5, 1, \dots$] by this Gaussian decaying function [Eq. (C1)], yielding the analytical results in Fig. 6(a). Furthermore, the decay of the coherence function for the kagome lattice shown in Fig. 6(b) was analytically calculated by finding the probability distribution of states that have relative phase differences of $\pm 2\pi/3$ or 0 with respect to the reference laser and was found to decay exponentially as $1/2^n$, where n denotes the distance from the reference laser.

APPENDIX D: STATISTICAL ANALYSIS

We performed a statistical analysis to quantify the agreement of our results with the predictions of ideal fair sampling. We started by obtaining the normalized coherence as a function of the number of realizations for NN and NNN and then calculated the standard deviation with respect to the theoretical values of coherences. Note that each realization consists of averaging over ~ 250 independent simulations, using 250 longitudinal laser modes. The results are presented in Fig. 11. As is evident, for NN lasers in a triangular lattice, the normalized coherence varies within the standard deviation of 5% [shown in Fig. 11(a)]. A similar variation is also observed for NNN lasers. For NN and NNN lasers in a kagome lattice, the normalized coherences vary within the standard deviations of 6% and 8%, respectively [as shown in Fig. 11(b)]. These analyses confirm that our results agree with the ideal fair sampling within a few percent of deviation from the theoretical values of coherence.

[1] C. H. Papadimitriou and K. Steiglitz, *Combinatorial Optimization: Algorithms and Complexity* (Dover, Mineola, NY, 1998).
 [2] Y. Yamamoto, K. Aihara, T. Leleu, K. Kawarabayashi, S. Kako, M. Fejer, K. Inoue, and H. Takesue, Coherent Ising machines—Optical neural networks operating at the quantum limit, *npj Quantum Inf.* **3**, 49 (2017).

[3] N. G. Berloff, M. Silva, K. Kalinin, A. Askitopoulos, J. D. Topfer, P. Cilibizzi, W. Langbein, and P. G. Lagoudakis, Realizing the classical xy Hamiltonian in polariton simulators, *Nat. Mater.* **16**, 1120 (2017).
 [4] P. G. Lagoudakis and N. G. Berloff, A polariton graph simulator, *New J. Phys.* **19**, 125008 (2017).

- [5] P. L. McMahon, A. Marandi, Y. Haribara, R. Hamerly, C. Lagrock, S. Tamate, T. Inagaki, H. Takesue, S. Utsunomiya, K. Aihara, R. Byer, M. M. Fejer, H. Mabuchi, and Y. Yamamoto, A fully programmable 100-spin coherent Ising machine with all-to-all connections, *Science* **354**, 614 (2016).
- [6] Y. Takeda, S. Tamate, Y. Yamamoto, H. Takesue, T. Inagaki, and S. Utsunomiya, Boltzmann sampling for an xy model using a non-degenerate optical parametric oscillator network, *Quantum Sci. Technol.* **3**, 014004 (2018).
- [7] M. Nixon, E. Ronen, A. A. Friesem, and N. Davidson, Observing Geometric Frustration with Thousands of Coupled Lasers, *Phys. Rev. Lett.* **110**, 184102 (2013).
- [8] V. Pal, C. Tradonsky, R. Chriki, A. A. Friesem, and N. Davidson, Observing Dissipative Topological Defects with Coupled Lasers, *Phys. Rev. Lett.* **119**, 013902 (2017).
- [9] T. Inagaki, K. Inaba, R. Hamerly, K. Inoue, Y. Yamamoto, and H. Takesue, Large-scale Ising spin network based on degenerate optical parametric oscillators, *Nat. Photonics* **10**, 415 (2016).
- [10] A. Marandi, Z. Wang, K. Takata, R. L. Byer, and Y. Yamamoto, Network of time-multiplexed optical parametric oscillators as a coherent Ising machine, *Nat. Photonics* **8**, 937 (2014).
- [11] M. S. Könz, G. Mazzola, A. J. Ochoa, H. G. Katzgraber, and M. Troyer, Uncertain fate of fair sampling in quantum annealing, *Phys. Rev. A* **100**, 030303(R) (2019).
- [12] S. Mandrà, Z. Zhu, and H. G. Katzgraber, Exponentially Biased Ground-State Sampling of Quantum Annealing Machines with Transverse-Field Driving Hamiltonians, *Phys. Rev. Lett.* **118**, 070502 (2017).
- [13] E. Farhi, J. Goldstone, S. Gutmann, J. Laplan, A. Lundgren, and D. Preda, A quantum adiabatic evolution algorithm applied to random instances of an NP-complete problem, *Science* **292**, 472 (2001).
- [14] M. Yamamoto, M. Ohzeki, and K. Tanaka, Fair sampling by simulated annealing on quantum annealer, *J. Phys. Soc. Jpn.* **89**, 025002 (2020).
- [15] J. A. Acebrón, L. L. Bonilla, C. J. P. Vicente, F. Ritort, and R. Spigler, The Kuramoto model: A simple paradigm for synchronization phenomena, *Rev. Mod. Phys.* **77**, 137 (2005).
- [16] V. Pal, C. Tradonsky, R. Chriki, G. Barach, A. A. Friesem, and N. Davidson, Phase locking of even and odd number of lasers on a ring geometry: Effects of topological-charge, *Opt. Express* **23**, 13041 (2015).
- [17] R. Chriki, S. Mahler, C. Tradonsky, V. Pal, A. A. Friesem, and N. Davidson, Spatiotemporal supermodes: Rapid reduction of spatial coherence in highly multimode lasers, *Phys. Rev. A* **98**, 023812 (2018).
- [18] S. Mahler, M. L. Goh, C. Tradonsky, A. A. Friesem, and N. Davidson, Improved Phase Locking of Laser Arrays with Nonlinear Coupling, *Phys. Rev. Lett.* **124**, 133901 (2020).
- [19] D. Mehuys, W. Streifer, R. G. Waarts, and D. F. Welch, Modal analysis of linear Talbot-cavity semiconductor lasers, *Opt. Lett.* **16**, 823 (1991).
- [20] C. Tradonsky, M. Nixon, E. Ronen, V. Pal, R. Chriki, A. A. Friesem, and N. Davidson, Conversion of out-of-phase to in-phase order in coupled laser arrays with second harmonics, *Photonics Res.* **3**, 77 (2015).
- [21] C. Tradonsky, V. Pal, R. Chriki, N. Davidson, and A. A. Friesem, Talbot diffraction and Fourier filtering for phase locking an array of lasers, *Appl. Opt.* **56**, A126 (2017).
- [22] M. Nixon, M. Fridman, A. A. Friesem, and N. Davidson, Enhanced coherence of weakly coupled lasers, *Opt. Lett.* **36**, 1320 (2011).
- [23] The vortex (antivortex) state is constructed by imposing the phases $(0, 2\pi/3, -2\pi/3)$ [$(0, -2\pi/3, 2\pi/3)$] on a certain triangle and then setting all other lasers in a unique manner to be separated by $\pm 2\pi/3$ from their nearest neighbors.
- [24] J. T. Chalker, P. C. W. Holdsworth, and E. F. Shender, Hidden Order in a Frustrated System: Properties of the Heisenberg Kagome Antiferromagnet, *Phys. Rev. Lett.* **68**, 855 (1992).
- [25] R. Moessner and J. T. Chalker, Low-temperature properties of classical geometrically frustrated antiferromagnets, *Phys. Rev. B* **58**, 12049 (1998).
- [26] For NN, the probabilities for a state to have a phase difference of either $+2\pi/3$ or $-2\pi/3$ or 0 are $P(+)=1/2$, $P(-)=1/2$, and $P(0)=0$. For NNN, the probabilities are $P(+)=1/4$, $P(-)=1/4$, and $P(0)=1/2$. For NNNN, the probabilities are $P(+)=3/8$, $P(-)=3/8$, and $P(0)=1/4$. In general, at a distance n from the reference laser, the coherence varies as $1/2^n$.
- [27] J. Li, J. Lee, W. Huang, S. Burchesky, B. Shteynas, F. C. Top, A. O. Jamison, and W. Ketterle, A stripe phase with supersolid properties in spinorbit-coupled Bose-Einstein condensates, *Nature (London)* **543**, 91 (2017).
- [28] C. Tradonsky, I. Gershenzon, V. Pal, R. Chriki, A. A. Friesem, O. Raz, and N. Davidson, Rapid laser solver for the phase retrieval problem, *Sci. Adv.* **5**, eaax4530 (2019).
- [29] J. W. Goodman, A. R. Dias, and L. M. Woody, Fully parallel, high-speed incoherent optical method for performing discrete Fourier transforms, *Opt. Lett.* **2**, 1 (1978).
- [30] H. J. Caulfield, D. Dvornik, J. W. Goodman, and W. Rhodes, Eigenvector determination by noncoherent optical methods, *Appl. Opt.* **20**, 2263 (1981).
- [31] A. G. Fox and T. Li, Resonant modes in a maser interferometer, *Bell Syst. Tech. J.* **40**, 453 (1961).
- [32] R. W. Gerchberg and W. O. Saxton, A practical algorithm for the determination of the phase from image and diffraction plane pictures, *Optik* **35**, 237 (1972).